Phase relaxation of photoexcited triplet spins in CaO

M. Glasbeek and R. Hond

Laboratory for Physical Chemistry, University of Amsterdam, Nieuwe Achtergracht 127, 1018 WS Amsterdam, The Netherlands

Spin dephasing in the photoexcited $^3B_1$ state of the F_2^{2+} center in CaO is investigated using techniques for optical detection of microwave-induced coherent transients. Measurements of the spin-echo decay were performed at different (low) temperatures and (low) magnetic field strengths. The spectral diffusion results give quantitative support for a model in which the dephasing is due to random modulation of the dipolar coupling between the excited $S = 1$ spins and F^+-center spins of $S = 1/2$. A projection operator formalism is used to treat the dipolar-induced dephasing. The theory also allows for the experimental determination of the F^+-center spin-dephasing rate. It appears that between 1 and 10 K the phenomenon of one-phonon assisted exchange narrowing occurs in the F^+-center spin ensemble.

I. INTRODUCTION

Since the early work of Mims *et al.*,[1] there have been numerous reports on the application of electron-spin-echo techniques to the study of spin-dephasing processes in magnetically dilute ionic solids.[2] In general, spin-spin interactions are of fundamental importance in the phase relaxation mechanisms. They contribute to observed phenomena as spin diffusion, cross-relaxation, and nuclear modulation effects.[3] For ionic crystals experimental efforts have, until recently, been focused on systems involving electronic ground-state spins only, thus leaving many important questions regarding the spin coherence decay in electronic excited states unexplored. Spin coherence studies of excited states in molecular crystals, on the other hand, have progressed rapidly in recent years. Especially investigations on photoexcited triplet states in organic crystals have proved to be of great value for exposing many of the details of intra- and intermolecular relaxation processes.[4] This study was undertaken in an attempt to obtain complementary information about spin dephasing in excited ionic solids.

From an experimental point of view, an attractive feature of photoexcited triplet states is their spin selective feeding and decay. As a consequence, at zero field and under conditions of suppressed spin-lattice relaxation, the spin alignment may become unusually large and therefore be of considerable advantage in coherent microwave spectroscopy. The detection sensitivity may increase even more when the investigated system allows for the use of optical methods for the detection of microwave resonance phenomena.[5] Double-resonance techniques of this kind have recently been shown to be of use in the study of photoexcited ionic solids.[6,7] In this paper we study one of these systems in more detail, namely F_2^{2+} centers

in their photoexcited $^3B_1$ state in CaO. In a preliminary report, the major results have been briefly discussed.[8] Here we want to give a more detailed account of the developed theory and the experimental data obtained.

At the low temperatures of our experiments, direct spin-phonon coupling does not contribute, neither by T_1- nor by T_2-type mechanisms, to the $^3B_1$-state spin dephasing (see below). Instead, the triplet spin dephasing is determined by the presence of abundant F^+ centers in the lattice, with a net spin of $S = \frac{1}{2}$. These F^+ centers undergo random spin flips which, by virtue of magnetic dipolar interactions with the excited triplet spins, produce a random modulation of the resonance frequencies of the latter. However, the triplet spin angular momentum when perturbed by a nonaxial symmetric crystal field becomes quenched in zero magnetic field, and hence it is anticipated that spectral diffusion based on modulated magnetic dipolar coupling is heavily reduced. Indeed, the phase memory time of F_2^{2+} centers in the $^3B_1$ state at zero field ($T_M \simeq 140$ μsec) is at least 1 order of magnitude longer than the electron-spin-dephasing times ordinarily measured for Kramers spin ensembles. Also, changes of the echo decay rate as a function of an applied external magnetic field will be of interest. Such effects have previously not been considered although they are related to those known in the field of nuclear magnetic resonance.[9,10] Here the specific effects of a magnetic field on the echo behavior of an electron-spin triplet will be treated in detail.

When the triplet spin coherence is determined by the dynamics of fluctuating $S = \frac{1}{2}$ spins, one usually distinguishes between T_1- and T_2-type samples where reference is made to the dominant dephasing mechanism in the $S = \frac{1}{2}$ spin bath. It is to be expected that at low temperatures and zero magnetic field the T_1-type processes are severely

suppressed. The experimental procedures of this work allow us to examine the role of pure dephasing processes (i.e., of T_2 type) in the phase relaxation of the F^+-center spin ensemble under such conditions. We find as a main result, from temperature- and magnetic-field-dependent measurements, that in the region between 1 and 10 K, the phenomenon of exchange narrowing takes place within the F^+-center ensemble.

The paper is outlined as follows: In Sec. II the theory is presented. For those readers not familiar with the methods for optical detection of spin coherence we briefly review the principles. Starting from the Von Neumann–Liouville equation, the equation of motion of the echo observable is derived in a straightforward manner. An analytical solution for its time evolution is obtained assuming the validity of a statistical averaging procedure and random modulation of the F^+-center spin frequencies. From the echo attenuation analysis a number of experiments emerge. Details of the experimental setup are given in Sec. III. The results associated with the experiments are presented and discussed in Sec. IV. This section also contains the results from cross-relaxation and spin-ordering experiments not dealt with before. The data provide insight in the extent of thermal isolation of the $^3B_1$-state sublevels and their involvement in energy-transfer processes.

II. THEORETICAL

A. Coherence formation

In an ensemble of two-level systems coherence phenomena may be observed when the two states β and γ are strongly coupled by an intense resonant radiation field and relaxation during excitation can be neglected. For triplet spins the two-level framework still holds as long as we consider the situation that the difference in resonance frequencies for the various possible transitions is very high compared to the Rabi frequency.[11] Using this approach we wish to find the operator associated with the coherence observable for an ensemble of identical triplet systems perturbed by a static magnetic field. The spin Hamiltonian for each triplet species is given as

$$\mathfrak{IC} = -XS_x^2 - YS_y^2 - ZS_z^2 + g\mu_\beta H_z S_z + V(t) = \mathfrak{IC}_0 + V(t),$$

$$(2.1)$$

where X, Y, and Z denote the zero-field energies in the spin sublevels, the magnetic field H_z is applied along the molecular principle z axis, and $V(t)$ gives the time-dependent interaction between the triplet state and the oscillating microwave field. The stationary eigenfunctions of the time-

independent Hamiltonian [i.e., $V(t) = 0$ in Eq. (2.1)] are labeled as α, β, and γ with a level ordering as in the inset of Fig. 1. By choosing the microwave frequency $\omega = \omega_{\beta\gamma}$ far off resonance from the α to β and the α to γ transition frequencies, we obtain in the α, β, γ basis

$$\mathfrak{IC} = \begin{pmatrix} E_\alpha & 0 & 0 \\ 0 & E_\beta & V_{\beta\gamma} \\ 0 & V_{\gamma\beta} & E_\gamma \end{pmatrix}.$$

$$(2.2)$$

The zero-valued off-diagonal elements result from rapid averaging out at frequencies far off resonance. It is apparent that V causes a superposition state, $\psi = p \, |\beta\rangle + q \, |\gamma\rangle$. Coherence arises because the off-diagonal elements of the density matrix become nonzero: $\rho_{\beta\gamma}, \rho_{\gamma\beta} \neq 0$, where $\rho_{\beta\gamma} = \overline{pq}^*$. Experimentally we obtain information about the spin coherence from phosphorescence intensity changes as induced by an applied microwave pulse sequence. For the probe techniques applied in this work it can be derived[5] [see also the discussion following Eq. (2.12)] that the optical intensity effects are described by the time behavior of a parameter, $r_1^*(t)$, which is expressed as

$$r_1^*(t) = \rho_{\beta\gamma}^* + \rho_{\gamma\beta}^*.$$

$$(2.3)$$

Here the density matrix elements are considered in the interaction representation (as indicated by the asterisk) and obtained from,
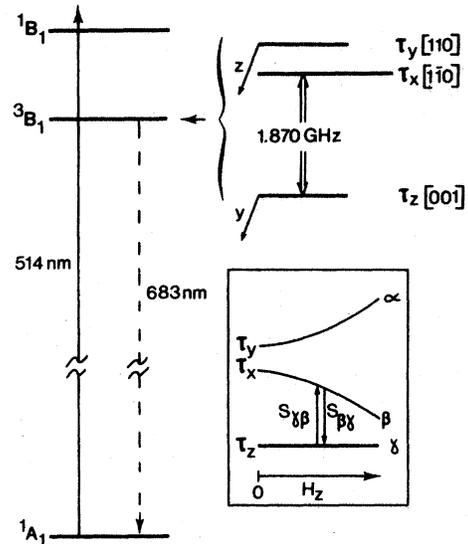
FIG. 1. Optical pumping cycle for probing coherence between the τ_z and τ_x spin levels of the F_2^{2+} center $^3B_1$ state in CaO. The triplet sublevel spacing is shown on an enlarged scale. The inset depicts the level splittings when a magnetic field is applied along the molecular z axis; $S_{\gamma\beta}$ and $S_{\beta\gamma}$ are raising and lowering operators for the transitions $\gamma \rightarrow \beta$ and $\beta \rightarrow \gamma$, respectively.

$$\rho^* = U\rho U^{-1} \, , \tag{2.4}$$

where

$$U = \exp(i\mathcal{H}_0 t) \, . \tag{2.5}$$

Throughout this paper we work in units where $\hbar = 1$. We now introduce the equivalent operator S_1 for the coherence observable by writing

$$r_1^* = \langle\langle S_1^* \rangle\rangle_{\mathrm{av}} = \mathrm{Tr}(\rho S_1^*) = \mathrm{Tr}(\rho^* S_1) \, , \tag{2.6}$$

where

$$S_1^* = U^{-1} S_1 U \, . \tag{2.7}$$

By equating (2.3) and (2.6) we obtain for the matrix representation of S_1 in the α, β, γ basis

$$S_1 = \begin{bmatrix} 0 & 0 & 0 \\ 0 & 0 & 1 \\ 0 & 1 & 0 \end{bmatrix} \, . \tag{2.8}$$

Since the raising and lowering operators for the spin transitions (cf. Fig. 1) are given by

$$S_{\beta\gamma} = \begin{bmatrix} 0 & 0 & 0 \\ 0 & 0 & 0 \\ 0 & 1 & 0 \end{bmatrix} \, , \quad S_{\gamma\beta} = \begin{bmatrix} 0 & 0 & 0 \\ 0 & 0 & 1 \\ 0 & 0 & 0 \end{bmatrix} \, , \tag{2.9}$$

etc, we also have

$$S_1 = S_{\beta\gamma} + S_{\gamma\beta} \, . \tag{2.10}$$

The result (2.10) will be of use in the formal treatment of the next section where the time development of $\langle\langle S_1^* \rangle\rangle_{\mathrm{av}}$ under the influence of randomly fluctuating perturbations is treated explicitly. However, we first wish to briefly recall some of the characteristics of coherence phenomena as viewed in the Feynman, Vernon, and Hellwarth (FVH) geometrical representation[12] in order to facilitate visualization of the various experiments of this work.

In the FVH model the precessional motion of a "pseudo" magnetization vector $\vec{r}$ about a field $\vec{\Omega}$ is considered. $\vec{r}$ and $\vec{\Omega}$ are specified by their projections along three orthogonal axes (e_1, e_2, e_3) in abstract space as follows:

$$\vec{r} = (r_1, r_2, r_3) = ((\rho_{\beta\gamma} + \rho_{\gamma\beta}), i(\rho_{\beta\gamma} - \rho_{\gamma\beta}), (\rho_{\beta\beta} - \rho_{\gamma\gamma})) \tag{2.11a}$$

and

$$\vec{\Omega} = (\Omega_1, \Omega_2, \Omega_3) = ((V_{\beta\gamma} + V_{\gamma\beta}), i(V_{\beta\gamma} - V_{\gamma\beta}), (E_\beta - E_\gamma)) \, . \tag{2.11b}$$

With neglect of relaxation the equation of motion for the density matrix can be transformed into[4]

$$\frac{d\vec{r}}{dt} = \vec{\Omega} \times \vec{r} \, . \tag{2.12}$$

The typical experiments of Sec. IV are the following.

(i) Optical detection of spin echo. Here the applied pulse cycle is $\pi/2\text{-}\tau\text{-}\pi\text{-}\tau\text{-}\pi/2$. From Eqs. (2.11) and (2.12) the behavior of the vector $\vec{r}(t)$ can now be constructed in the interaction representation. The first $\pi/2$ pulse causes a tilt of r_3^* about the e_2 axis over $90°$ into the $e_1\text{-}e_2$ plane, whereby the initially incoherent ensemble $[\vec{r}(0) = r_3(0)]$ develops into a coherent ensemble $[r_1^*(t) \neq 0]$. In the time interval from 0 to τ a free-induction decay occurs because not all of the spins have the same resonance frequency (inhomogeneous broadening). The π pulse restores the r_1^* component at 2τ whereas the final $\pi/2$-probe pulse rotates $r_1^*(2\tau)$ about e_2 until it is aligned along e_3. In the optical region this microwave pulse sequence is accompanied by changes in the intensity of the emission from the excited triplet state. These intensity effects, however, can arise only because of the difference in the emissive properties of the β and γ levels and the microwave-induced effects on the population distribution among these levels (i.e., changes of the r_3 component). Changes in the r_1^* and r_2^* components, on the other hand, are not directly reflected in the phosphorescence intensity. For this reason the final $\pi/2$ pulse is applied, which accomplishes a conversion of the coherence component into the detectable r_3 component.

(ii) Optical detection of spin ordering. In this experiment one wants to study the fate of a spin ensemble of which the individual spins are aligned in their own local field. The alignment (ordering) is performed in the following way.[13,14] A $\pi/2$ pulse rotates the r_3 component along e_1. The resultant r_1^* component is immediately spinlocked to the microwave H_1 field by phase shifting the latter over $90°$. More precisely, the locking of each spin packet is to its effective local field, which is defined as the vector sum of H_1 and the shift of the packet in the rotating frame, $\Delta\omega_i$; $\Delta\omega_i$ is directed along e_3 [cf. Eq. (2.11b)]. By a gradual reduction of H_1 to zero, the "pseudo" magnetization of each spin adiabatically follows the reorientation of the effective local field until it is aligned along $+e_3$ (for $\Delta\omega_i > 0$) or $-e_3$ (for $\Delta\omega_i < 0$). The ordered state decays[14,15] owing to spin-lattice relaxation, spin energy-transfer processes that involve a limited local-field lifetime (e.g. cross-relaxation), etc. The residual ordering is measured in a modified Hahn echo experiment for which the pulse sequence is taken as $(\pi/2, 0°)\text{-}\tau\text{-}(\pi, 0°)\text{-}\tau'\text{-}(\pi/2, 90°)$. Reasoning as above, as a result of the first two pulses, a transverse r_2 component is built up with an amplitude that develops during the time interval τ' as the shape function of Fig. 11. A plot of the peak to peak height versus the order-

ing time τ_0 yields the characteristic spin-ordering decay time.

B. Coherence decay

Several spin-dephasing theories have been advanced,[16,17,18] all of which treat so-called T_1 samples. The basic assumption is that random modulation of the transition frequencies in the coherent ensemble (consisting of A spins) arises because of magnetic dipolar contact with B spins which in turn undergo stochastic flipping due to spin-lattice relaxation. Instead of applying the density-matrix formalism as for T_1 samples, we prefer to present the derivation in Liouville space because this approach allows us to point out to what extent T_1 and T_2 samples can be treated on equal footing.

Here the specific situation is considered of the A spins being in the excited triplet state, whereas the B spins are $S = \frac{1}{2}$ spins in their electronic ground state. The many-particle spin system is characterized by

$$\mathfrak{K} = \mathfrak{K}_0^A + \mathfrak{K}_{DD}^{AB} + \mathfrak{K}^B,\tag{2.13}$$

where

$$\mathfrak{K}_0^A = \sum_{A\text{ spins}} [-X(S_x^A)^2 - Y(S_y^A)^2 - Z(S_z^A)^2 + g_A \mu_B H_z S_z^A]\tag{2.14a}$$

and

$$\mathfrak{K}_{DD}^{AB} = g_A g_B \mu_B^2 \sum_{A,B\text{ spins}} \frac{1}{r_{AB}^3}\left(\vec{S}_A \cdot \vec{S}_B - \frac{3(\vec{S}_A \cdot \vec{r}_{AB})(\vec{S}_B \cdot \vec{r}_{AB})}{r_{AB}^2}\right).\tag{2.14b}$$

$\mathfrak{K}^B$ contains all the B-spin interactions except for the coupling between A and B spins. Since $\mathfrak{K}^B$ comprises noncommutative terms, its spin operators are time dependent. They are considered as being stochastically modulated and consequently cause fluctuations in $\mathfrak{K}_{DD}^{AB}$.

The time development of the density matrix in the A-spin interaction representation is given by

$$\frac{\partial \rho^*}{\partial t} = i[\rho^*, \mathfrak{K}^*],\tag{2.15}$$

where

$$\mathfrak{K}^* = U\mathfrak{K}U^{-1} + i\frac{\partial U}{\partial t}U^{-1} = U\mathfrak{K}_{DD}^{AB}U^{-1} + \mathfrak{K}^B,\tag{2.16}$$

for $U = \exp(i\mathfrak{K}_0^A t)$. Combining Eqs. (2.6) and (2.15) yields

$$\left\langle \frac{\partial \langle S_1^* \rangle}{\partial t} \right\rangle_{av} = -i\,\text{Tr}(S_1[\mathfrak{K}^*, \rho^*]),\tag{2.17}$$

where

$$S_1 = \sum_{A\text{ spins}} (S_{\beta\gamma}^A + S_{\gamma\beta}^A).\tag{2.18}$$

Henceforth we will use the notation customary for the operator representation in Liouville space.[19] We write

$$(A|B) = \text{Tr}(A^\dagger B),$$

$A^\dagger$ being the adjoint of A. Liouville operators operate in a space spanned by Hilbert operators and are written as

$$\hat{\Theta}A = [\Theta, A],$$

and

$$e^{-i\hat{\Theta}t}A = e^{-i\Theta t}Ae^{i\Theta t}.$$

Thus Eq. (2.17) can be rewritten as

$$\left\langle \frac{\partial \langle S_1^* \rangle}{\partial t} \right\rangle_{av} = -i(S_1|\hat{\mathfrak{K}}^*|\rho^*).\tag{2.19}$$

With the introduction of the projection (super)operator P, so that

$$|\rho) = P|\rho) + (1-P)|\rho),\tag{2.20}$$

one obtains after some operator algebra[20] the generalized equation of motion:

$$\left\langle \frac{\partial \langle S_1^*(t) \rangle}{\partial t} \right\rangle_{av} = -i(S_1|\hat{\mathfrak{K}}^*P|\rho^*) - i(S_1|\hat{\mathfrak{K}}^*S(t,0)(1-P)|\rho^*(0)) - \int_0^t dt'(S_1|\hat{\mathfrak{K}}^*(t)S(t,t')(1-P)\hat{\mathfrak{K}}^*(t')P|\rho^*(t')),\tag{2.21}$$

where the propagator $S(t, t')$ is

$$S(t, t') = T\exp\left(-i\int_{t'}^t d\tau(1-P)\hat{\mathfrak{K}}^*(\tau)\right)\tag{2.22}$$

and T is the Dyson time-ordering operator[21] which orders operators with greater time arguments to the left-hand side. In the echo decay experiment we are interested in the time evolution of $\langle\langle S_1^*(t)\rangle\rangle_{av}$. Projection on a subspace defined by

$$P = \frac{|S_1)(S_1|}{(S_1|S_1)}\tag{2.23}$$

is therefore required. Immediately after the first $\pi/2$ pulse at $t = 0$ one has

$$|\rho^*(0)) \propto |S_1).\tag{2.24}$$

Substitution of Eqs. (2.23) and (2.24) into Eq. (2.21) leads to

$$\left\langle \frac{\partial \langle S_1^*(t) \rangle}{\partial t} \right\rangle_{av} = - \int_0^t dt' (S_1 | \hat{\mathfrak{X}}^*(t) S(t,t')(1-P)\hat{\mathfrak{X}}^*(t')P | \rho^*(t')). \qquad (2.25)$$

In a Magnus expansion[22] the propagator $S(t,t')$ is written as

$$S(t,t') = T \exp[-i(1-P)F(t-t')] = \exp[-i(1-P)(\bar{\mathfrak{X}}^* + \mathfrak{X}^{*(1)} + \bar{\mathfrak{X}}^{*(2)} + \cdots)(t-t')], \qquad (2.26)$$

where

$$\bar{\mathfrak{X}}^* = \frac{1}{t_c} \int_0^{t_c} \mathfrak{X}^*(\tau) d\tau, \quad t_c = t - t'. \qquad (2.27)$$

$\bar{\mathfrak{X}}^{*(n)}$ (the nth term in the Magnus iteration procedure) is here taken to be zero for $n \geq 1$ (i.e., the lowest Born approximation is applied). For $t_c \gg \tau_c$, τ_c being the characteristic correlation time of the fluctuations that cause the time dependence of the B spins, $\bar{\mathfrak{X}}^*$ averages to zero and Eq. (2.25) becomes

$$\left\langle \frac{\partial \langle S_1^*(t) \rangle}{\partial t} \right\rangle_{av} = - \int_0^t dt' K(t) \langle\langle S_1^*(t') \rangle\rangle_{av}, \qquad (2.28)$$

where the kernel

$$K(t) = \frac{(S_1 | \hat{\mathfrak{X}}^*(t)(1-P)\hat{\mathfrak{X}}^*(t') | S_1)}{(S_1 | S_1)} \qquad (2.29)$$

represents the memory function in lowest order.

$K(t)$ may now be evaluated using Eqs. (2.16) and (2.23). Those terms in $\mathfrak{X}_{DD}^{AB}$ that do not commute with $\mathfrak{X}_0^A$ are rapidly averaged out and thus need not be considered in $\mathfrak{X}^*$, only the secular part of $\mathfrak{X}_{DD}^{AB}, \mathfrak{X}_{DD}^{AB}(\text{sec})$ is retained. Also, we restrict ourselves to nonresonant magnetic dipolar interactions between A and B spins, i.e., we consider only $[\mathfrak{X}_0^A, \mathfrak{X}_{DD}^{AB}(\text{sec})] = 0$, but not the possibility of $[\mathfrak{X}_0^A, \mathfrak{X}_{DD}^{AB}] = -[\mathfrak{X}_0^B, \mathfrak{X}_{DD}^{AB}] = \pm \omega_0 \mathfrak{X}_{DD}^{AB}$. The latter relations are relevant to cross relaxation between A and B spins. Special effects due to the resonant coupling between A and B spins, as achieved for certain values and orientations of the externally applied magnetic field, have been observed in the spin-echo decay behavior of the A spins and will be discussed in a future publication.[23] As proved in Appendix A, here $\mathfrak{X}_{DD}^{AB}(\text{sec})$ simply becomes

$$\mathfrak{X}_{DD}^{AB}(\text{sec}) = g_A g_B \mu_B^2 \sum_{A,B} \frac{z}{(1+z^2)^{1/2}} \frac{1 - 3Z_{AB}^2}{r_{AB}^3} S_{zA} S_{zB}, \qquad (2.30)$$

where Z_{AB} is the direction cosine of r_{AB} with respect to the z axis of the A spin fine-structure tensor, $z = g_A H_z' |E|^{-1}$, $H_z' = (H_{loc}^2 + H_z^2)^{1/2}$, H_{loc} being the effective local field at A-spin sites and, finally,

$$S_{sA} = \frac{z}{(1+z^2)^{1/2}} S_{zA} + \frac{1}{2(1+z^2)^{1/2}} [(S_{+A})^2 + (S_{-A})^2], \qquad (2.31)$$

or in the α, β, γ matrix representation,

$$S_{sA} = \begin{bmatrix} 1 & 0 & 0 \\ 0 & -1 & 0 \\ 0 & 0 & 0 \end{bmatrix}. \qquad (2.32)$$

To calculate the memory function, $K(t)$, we assume uncorrelated A and B spins for which the many-particle spin eigenfunction is a simple product of the individual A and B spin functions. Within this approach $K(t)$ is readily calculated by substitution of Eq. (2.30) in Eq. (2.29). We find

$$K(t) = \sum_{A,B} a_{AB}^2 \frac{\text{Tr}_B[S_{zB}(t) S_{zB}(t')]}{\text{Tr}_B} \frac{1}{n_A}, \qquad (2.33)$$

where

$$a_{AB} = g_A g_B \mu_B^2 \frac{1 - 3Z_{AB}^2}{r_{AB}^3} \frac{z}{(1+z^2)^{1/2}},$$

n_A is the number of A spins and Tr_B is the trace of the unit operator in the subspace of a single B spin. In the high-temperature approximation one has $\mathfrak{X}^B \gg kT$, and the time autocorrelation function, $C_B(t,t')$, for the S_{zB} operator in the canonical ensemble of B spins can be written as

$$C_B(t,t') = \text{Tr}_B[\rho_B S_{zB}(t) S_{zB}(t')] \simeq \frac{\text{Tr}_B[S_{zB}(t) S_{zB}(t')]}{\text{Tr}_B}. \qquad (2.34)$$

Therefore Eq. (2.28) becomes

$$\left\langle \frac{\partial \langle S_1^*(t) \rangle}{\partial t} \right\rangle_{av} = -g_A^2 g_B^2 \mu_B^4 \int_0^t dt' \sum_{A,B} \frac{(1 - 3Z_{AB}^2)^2}{r_{AB}^6} \frac{z^2}{1+z^2} \frac{1}{n_A} C_B(t,t') \langle\langle S_1^*(t') \rangle\rangle_{av} \qquad (2.35)$$

At this point in the derivation one can distinguish between T_1 and T_2 samples if the dominant mechanism (T_1 or T_2) for the time development of $C_B(t,t')$ is known. As argued in Sec. IV, for our system it is concluded that not only the A spins lose coherence due to secular dipolar coupling with stochastically varying B spins, but the same is true for the B spins, i.e., we classify the sys-

tem as a T_2 sample. An explicit form for $C_B(t,t')$ is difficult to assess without exact knowledge of the origin and statistical behavior of the B-spin resonance frequency modulations. For illustrative purposes we consider in Appendix B the autocorrelation function for the simplified case of exchange narrowing between just two B-spin subgroups having slightly different resonance frequencies. In a more realistic model the problem is complicated because of the continuous spread in resonance frequencies and exchange scattering rates. On the other hand, for the physically appealing situation where the B-spin frequency distribution can be considered as Gaussian, it is permissable to represent $C_B(t,t')$ by a single exponential decay provided τ_c, the correlation time of the B-spin fluctuations, is short compared to the second moment of the spin-phonon interaction.[24] Hence assuming the applicability of the exchange narrowing limit we can write

$$C_B(t,t') = \langle S_{zB}^2(0) \rangle \exp(-R\,|t-t'|)\,, \qquad (2.36a)$$

where $\langle S_{zB}^2(0) \rangle = \frac{1}{4}$ for $S = \frac{1}{2}B$ spins and R denotes the B-spin dephasing rate.

Now $C_B(t,t')$ has the functional form of a correlation function in a Gauss-Markoff model. Note that Markoffian modulation of the B-spin resonance frequency is not relevant when the B spins dephase due to Heisenberg exchange interactions since it would lead to an infinite fourth moment of the B-spin spectral density.[22] However, for the situation where spin-phonon coupling is responsible for dephasing, Markoffian modulation of the B-spin resonances can not be excluded *a priori*

On the assumption that the decay rate of $\langle S_1^*(t') \rangle$ is small compared to that for the B-spin autocorrelation function in the interval $0 < t' < 2\tau$, Eq. (2.35) can be integrated to yield,

$$\langle\langle S_1^*(2\tau) \rangle\rangle_{av} \propto \exp\left(- \sum_{A,B} \frac{a_{AB}^2}{4} \frac{1}{n_A} \int_0^{2\tau} dt \int_0^t dt'\, s(t)s(t') \exp(-R\,|t'-t|)\right) = \exp\left(- \sum_{A,B} \frac{a_{AB}^2}{4} \frac{1}{n_A} B(\tau)\right), \qquad (2.36b)$$

where $s(t)$ is the function introduced by Klauder and Anderson[16] which takes into account the phase reversal at time τ in the echo experiment, i.e., $s(t) = +1$ for $t < \tau$, and -1 for $t > \tau$ and furthermore,

$$B(\tau) = 2R^{-2}\{R\tau - [1 - \exp(-R\tau)] - \tfrac{1}{2}[1 - \exp(-R\tau)]^2\}\,.$$
$$(2.36c)$$

For *dilute* samples in which the A and B spins are distributed at random in the lattice, Eq. (2.36b) can be further evaluated by invoking a well known statistical averaging procedure.[25]

Rewriting Eq. (2.36b) yields

$$\langle\langle S_1^*(2\tau) \rangle\rangle_{av} \propto \left(\prod_A \prod_B \exp\left(-\tfrac{1}{4}\,a_{AB}^2\right)\right)^{B(\tau)/n_A}\,. \quad (2.37)$$

Both A and B spins may occupy any point in space, thus a certain A-B pair contributes on the average to Eq. (2.37)

$$\langle S_{AB} \rangle = \left(\frac{1}{V} \int^V dV_{AB}\exp\left(-\tfrac{1}{4}\,a_{AB}^2\right)\right)^{B(\tau)/n_A} \quad (2.38)$$

because the A spin has a probability dV_{AB}/V of being in a volume element dV_{AB}. Evidently, $\langle S_{AB} \rangle$ is independent of which A spin we pick and hence,

$$\langle\langle S_1(2\tau) \rangle\rangle_{av} \propto \prod_B \langle S_{AB} \rangle^{n_A} = \langle S_{AB} \rangle^{n_A n_B}\,, \qquad (2.39)$$

where n_B is the number of B spins involved in the magnetic dipole-dipole interaction with the A spins. From Eqs. (2.38) and (2.39) we obtain

$$\langle\langle S_1^*(2\tau) \rangle\rangle_{av}$$

$$\propto \left[1 - \frac{n_B}{n_B}\left(1 - \frac{1}{V} \int^V dV \exp[-\tfrac{1}{4}\,a_{AB}^2\,B(\tau)]\right)\right]^{n_B}$$

$$= \left(1 - \frac{d_B}{n_B} \int^V dV\{1 - \exp[-\tfrac{1}{4}\,a_{AB}^2\,B(\tau)]\}\right)^{n_B}\,,$$
$$(2.40)$$

where d_B, the density of B spins, is equal to n_B/V. For n_B and V approaching infinity $\langle\langle S_1^*(2\tau) \rangle\rangle_{av}$ becomes

$$\langle\langle S_1^*(2\tau) \rangle\rangle_{av} \propto \exp\left(-2\pi d_B \int_0^\infty dr_{AB} \int_0^\pi d\theta_{AB} r_{AB}^2 \sin\theta_{AB}\{1 - \exp[-\tfrac{1}{4}a_{AB}^2 B(\tau)]\}\right)\,. \qquad (2.41)$$

Using

$$\int_0^\infty dx[1 - \exp(-x^{-2})] = \sqrt{\pi}$$

and

$$\int_{-1}^{+1} d(\cos\theta)\,|1 - 3\cos^2\theta\,| = (8\sqrt{3}/9)\,,$$

we obtain the final result

$$\langle\langle S_1^*(2\tau) \rangle\rangle_{av}$$

$$\propto \exp\left(-\frac{8\sqrt{3}}{27}\,\pi^{3/2} d_B g_A g_B \mu_B^2 \frac{z}{(1+z^2)^{1/2}}B(\tau)^{1/2}\right)\,.$$
$$(2.42)$$

III. EXPERIMENTAL

Our experimental setup for measuring optically detected magnetic resonance (ODMR) and spin coherence transients has been described in a previous paper.[7] Here we merely mention changes and additional facilities.

Optical excitation of a yellow-colored single crystal of CaO was by means of the 514-nm line from a Coherent Radiation CR-5 Ar^+ ion laser. To prevent unnecessary heating of the sample (this being immersed in a He bath or mounted in a He-flow cryostat), care was taken that the excitation power did not exceed ~25 mW. In experiments where magnetic field effects on the total phosphorescence intensity were investigated, use was made of superconducting Helmholtz coils which were immersed in the He bath and fed by a regulated power supply. Fields up to ~3 kG could then be realized. By amplitude modulation of the applied field (modulation amplitude was 5 G at $\nu \sim 30$ Hz) and appropriate lock-in detection, the effects of cross relaxation on the emitted light intensity in an external field could be probed sensitively.

Optical detection of spin coherence transients was essentially as before[6,7]; only slight modifications were introduced in the modes for microwave pulse generation and phase-sensitive lock-in detection of the light changes. The block diagram of Fig. 2 illustrates the components of the versatile pulse generator we used for driving the p-i-n diodes in the microwave circuit.[26] Prior to each spin-echo or spin-ordering experiment, a transient nutation was performed in order to establish the pulse width of a $\pi/2$ or π pulse. To this end the p-i-n diodes were driven by pulses of 30-Hz repetition frequency and of duration progressing linearly with time. These pulses were obtained from a monostable multivibrator which was triggered by the 30-Hz external reference of the synthesizer and which released pulses of increasing duration because it was swept by an analog ramp (from 0 to 5 V at a rate of 0.5 μsec/V). The light changes, induced synchronously with the resonant-microwave pulses, were phase-sensitive detected and exhibited, as readily visualized within the FVH model, oscillatory behavior. The first extremum is observed when population inversion occurs and determines the π-pulse duration time.

The echo-decay pulse sequence was obtained as follows. The digital ramp of a Varian C-1024 time-averaging computer was used to sweep the time separation between successive pulses from a 20-MHz clock oscillator. The resulting pulses were fed into a programmable synthesizer which consists of down counters and a series of monostable multivibrators. Triggered at 30 Hz by an
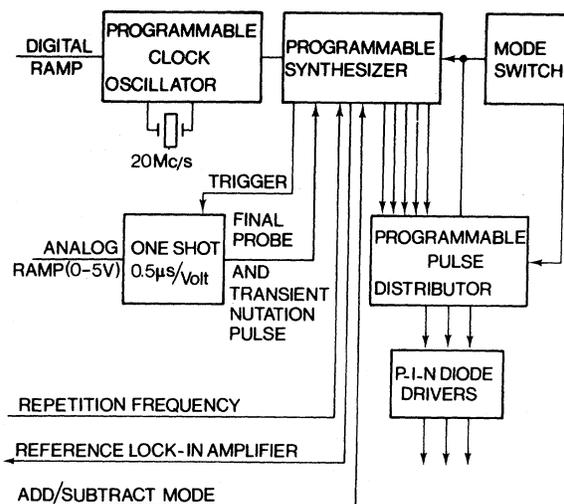
FIG. 2. Block scheme for the generation of the microwave pulse sequences.

external oscillator, the counter selected a preset number of pulses (n). In addition to these (n) pulses, the counter released an envelope pulse with overall width equal to the width of an (n)-pulse sequence. The two edges of the envelope pulse triggered $\pi/2$ pulses in one of the monostable multivibrators, whereas the n-pulse train triggered n π pulses in another monostable multivibrator. Finally, the pulses were combined in AND-OR gates and distributed to the p-i-n diode driver of a single microwave channel.

Especially for long times 2τ, one cannot use the reference pulse of the lock-in amplifier as the external oscillator for the synthesizer because the growing phase difference between the microwave-induced nonequilibrium phosphorescence intensity and the internal reference of the amplifier would make lock-in detection meaningless. To circumvent this problem, the lock-in amplifier reference was triggered synchronously with the final $\pi/2$ pulse of the synthesizer. Moreover, for long pulse sequences 2τ, population decay due to the limited triplet lifetime (3 msec) will also contribute to the echo decay. The measured echo-decay signal was corrected for this effect by repeating the experiment but now with the final $\pi/2$-probe pulse delayed by 1 μsec. The echo decay obtained in this way was subtracted from the previous one. Eventually, signal averaging was performed by accumulating alternately an "added" and "subtracted" signal.

Spin ordering was obtained by an initial $(\pi/2, 0°)$ microwave pulse followed by a 90° phase-shifted spin-locking pulse which existed for about 100 μsec, whereafter the microwave power was

gradually reduced to zero (see inserts of Figs. 11 and 12). In these experiments the two phase-shifted microwave channels were driven as follows. The 30-Hz external oscillator triggered in the synthesizer two monostable multivibrators, one of which delivered the $\pi/2$ pulse whereas the other produced a $\tau_1 \simeq 100$ μsec pulse. The falling edge of the latter was used to trigger yet another monostable multivibrator. Depending on the type of experiment (either detection of ordering, cf. Fig. 11 or ordering decay, Fig. 12) the latter multivibrator yielded a pulse of fixed duration or a pulse of which the width could be swept continuously. The trailing edge of this pulse triggered an (RC) network connected to the $p\text{-}i\text{-}n$ diode driver of the 90° channel so that the driver was loaded in about 100 μsec. The $\pi/2$ pulse was connected to the $p\text{-}i\text{-}n$ diode driver of the 0° channel, whereas the τ_1 and RC pulses were connected to the 90° channel. Finally, by means of a modified Hahn-echo experiment, using methods similar to those described above, the ordering and its decay could be detected.

IV. RESULTS AND DISCUSSION

A. Steady-state experiments

The magnetic and optical properties of the photoexcited $^3B_1$ state of the F_2^{2+} center in yellow-colored CaO have been discussed recently.[7] The defect is characterized by two electrons trapped at the sites of two neighboring oxygen anion vacancies along a $\langle 110 \rangle$ direction of the fcc crystal. Figure 1 summarizes the main spectroscopic data. On photoexcitation of the $^3B_1$ level at liquid-helium temperatures spin alignment is observed and therefore spin-lattice relaxation can be ignored. This and the selective radiative decay could be employed when establishing the existence of spin-spin interactions between F_2^{2+} centers and abundant F^+ centers (with $S = \frac{1}{2}$). The experiment is to measure cross-relaxation (CR) effects on the phosphorescence intensity for magnetic field strengths where F_2^{2+} centers become resonant with spin species of a different spin temperature.

Figure 3 shows the derivative of the intensity changes of the no-phonon line corresponding with the $^3B_1 \rightarrow {}^1A$ transition at (683 nm) as a function of $\vec{H}$ along the [010] crystal axis. Lines X and Y are characterized by a σ-polarized light increase and a π-polarized light decrease, which shows that the spin alignment among the β and γ levels becomes erased. The orientation dependence of the X peak (cf. Fig. 4) is in agreement with a simulation for CR between the $^3B_1$ state and an $S = \frac{1}{2}$ species with $g = 2.000 \pm 0.001$. F^+ centers are the most abundant $S = \frac{1}{2}$ defects. Clearly the X peak can be as-
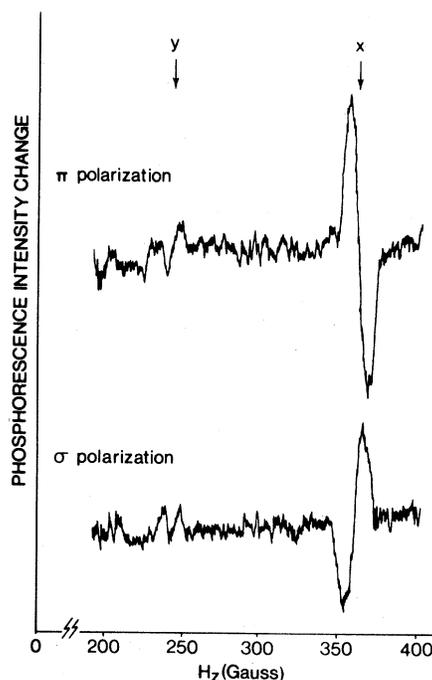
FIG. 3. Derivative of the variation in the phosphorescence intensity (detection wavelength 683 nm) as a magnetic field $\vec{H}$, along the [010] crystal axis, is swept; $T = 1.2$ K. The sharp changes reflect cross relaxation with F^+ centers.

signed to resonant coupling between F_2^{2+} and F^+ centers. Whereas the X peak in Fig. 3 involves a single spin-flip transition in both spin species ($\beta \rightarrow \gamma$ in F_2^{2+} centers vs $-\frac{1}{2} \rightarrow +\frac{1}{2}$ in F^+), the Y peak is interpreted as a single spin flip in the F_2^{2+} center ($\beta \rightarrow \gamma$) and a simultaneous spin flip in *two* F^+ centers. Multiple spin flips are higher-order processes and their presence definitely reflects a high F^+-center concentration. This result, put in a more quantitative basis in Sec. IV B, is of great relevance to the observed exchange narrowing phenomena discussed later.

B. Optically detected spin-echo decay

To observe spin coherence involving only the $\beta \rightarrow \gamma$ transition of Fig. 1, a magnetic field along the [010] crystallographic direction was applied of large enough magnitude to resolve the transition in normal ODMR. At lower fields where the microwave responses of differently oriented F_2^{2+} sites overlap, the light changes associated with the $\beta \rightarrow \gamma$ transition could be resolved by using a linear polarizer in the detection pathway for filtering [001] polarized emission. Spin-echo relaxation curves were obtained by measuring the optical response to a $\pi/2\text{-}\tau\text{-}\pi\text{-}\tau\text{-}\pi/2$ resonant microwave pulse sequence as a function of 2τ. Illustrative re-
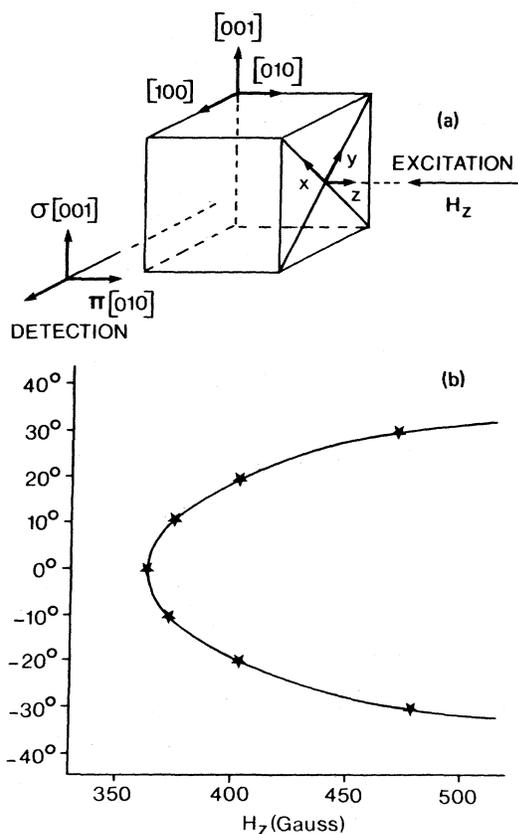
FIG. 4. (a) Directions of magnetic field, optical excitation and detection with respect to the CaO crystal main axes as used in the steady-state and spin-coherence experiments. One of the six possible orientations of the F_2^{2+}-center molecular axes is also shown. (b) Variation of the cross-relaxation peak (denoted as X in Fig. 3) upon rotation of the crystal about the [001] crystal axis (crosses denote experimental results). Drawn curve is computed for the case of cross relaxation between the F_2^{2+} center in its $^3B_1$ state and an $S = \frac{1}{2}$ spin species with $g = 2.000 \pm 0.001$.

sults for various values of temperature (T) and magnetic field strength (H_z) are presented in Figs. 5 and 6.

Phenomenologically, the echo decay curves could be fitted to functions of the form,[3]

$$E(2\tau) \propto \exp[(-2\tau/T_M)^x] , \qquad (4.1)$$

where $E(2\tau)$ is the optically detected echo amplitude measured as a function of τ, and T_M is some characteristic decay time. The variation of T_M and x with H_z is shown in Fig. 7. It is seen that the phase relaxation appears almost exponential in the presence of the magnetic field and also that T_M decreases by almost a factor of 4 when H_z is increased from zero up to 60 G. From Fig. 5 it is also noted that as T is increased, the echo de-
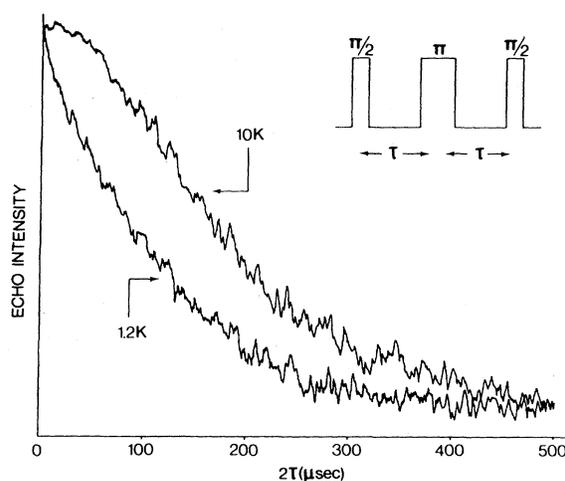
FIG. 5. Optically detected spin-echo decay curves of the F_2^{2+} center in CaO as monitored for the $|D\text{-}E|$ transition (at zero field) at 1.2 and 10 K, respectively.

cay curve attains a pronounced nonexponential shape. The plots of Fig. 8 express this in a more quantitative way; as T is increased x increases until at 10 K, $x = \frac{3}{2}$. Furthermore, T_M, which to a certain extent is still a measure for the phase memory time, increases as T is increased, or in other words, phase relaxation within the ensemble of $^3B_1$ spins slows down as the temperature is raised in the region from 1.2 to 10 K.

In considering the mechanism for dephasing we first remark that in general

$$T_M^{-1} = (T_2^*)^{-1} + (2T_1)^{-1} , \qquad (4.2)$$

where T_1 is the spin-lattice relaxation time associated with population relaxation and T_2^* is the
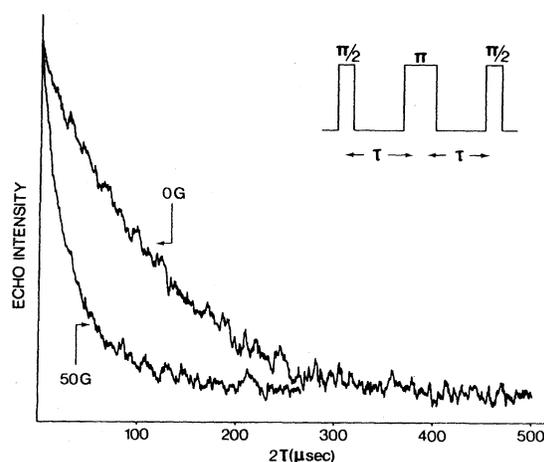
FIG. 6. Optically detected spin-echo decay curves of the F_2^{2+} center in CaO as monitored for the $\beta \rightarrow \gamma$ transition at 0 and 50 G, respectively ($T = 1.2$ K).
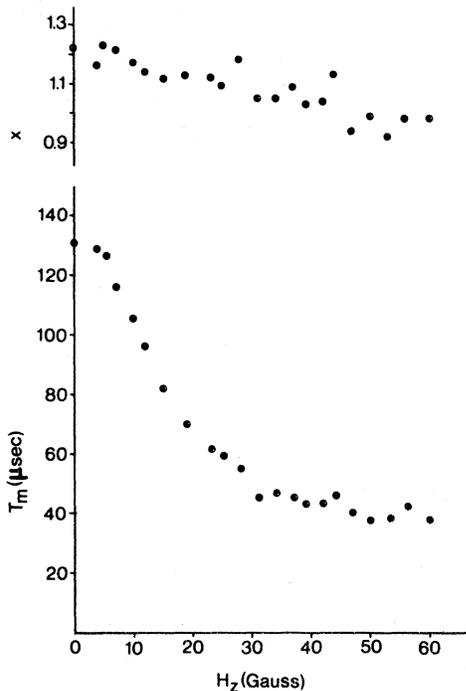
FIG. 7. Magnetic field dependence of the parameters T_m and x as determined by fitting the monitored spin-echo decay curves (for the $\beta \rightarrow \gamma$ transition at 1.2 K) to the form $\exp[-(2\tau/T_m)^x]$.

FIG. 8. Temperature dependence of the parameters T_m and x obtained by fitting the experimental spin-echo decay curves (at zero field) to the form $\exp[-(2\tau/T_m)^x]$.

characteristic "pure" dephasing time. Remember that T_1 and T_2^*, when determined by direct spin-phonon coupling,[27] would always show a decrease on a temperature rise. Apparently the decrease in T_M when T is increased from 10 K up to 15 K (cf. Fig. 8) is due to the A-spin spin-lattice coupling. However, experimentally a phonon-assisted slowing down of T_M is observed upon warming from 1.2 up to 10 K. Occurrence of this phenomenon eliminates direct spin-phonon coupling as a (pure) dephasing mechanism; the result can only be explained on the basis of exchange narrowing. This conclusion is further substantiated in Sec. IV C, where it is demonstrated that T_1 processes do not take place during the $^3B_1$ state lifetime on a microsecond time scale. Thus it remains to establish (i) what transitions are involved in the exchange narrowing processes, (ii) how does the coupling to the phonon reservoir come into play, and (iii) can we account for the observed effects of T and H_z in a more quantitative way.

One can conceive the lengthening of T_M with T to arise in a variety of ways. Firstly, the line narrowing could result from the averaging out of inhomogeneous broadening of only F_2^{2+} triplet spin transitions by either intra- or intermolecular dynamical exchange processes. For excited

molecular crystals, for instance, such exchange phenomena were proved to be of significant importance for spin dephasing.[4] Alternatively, the F_2^{2+} triplet spins could be magnetic dipolar coupled to another spin ensemble, which in turn exhibits motional averaging and which imposes a random modulation on the dipolar interactions. Again we use the argument of Sec. IV C where it is proved that the individual $^3B_1$ sublevels persist for at least milliseconds. Hence the $^3B_1$ state cannot possibly be involved in rapid exchange processes, and the former possibility can be dropped. Independent proof for the latter (dipolar) coupling mechanism is obtained from the analysis of the drastic influence of H_z on T_M, as discussed now.

In the model the shortening of the echo decay rate due to H_z is represented by Eq. (2.42). To determine whether this equation is followed the observed echo amplitude decays were computer fitted to the functional form, $\exp[-C(z)B(\tau)]$, where $B(\tau)$ is given by Eq. (2.36c). The procedure yielded a set of two parameters, $C(z)$ and R, as a function of the external variable H_z. Figure 9 plots the variation of C with H_z as evaluated from experiment. There is excellent agreement with the behavior predicted by the model. Note also the effect of H_z on R, the B-spin dephasing rate. A best-fit simulation shows $R \propto H_z^2$.

A T_1-type relaxation as the cause for B-spin de-
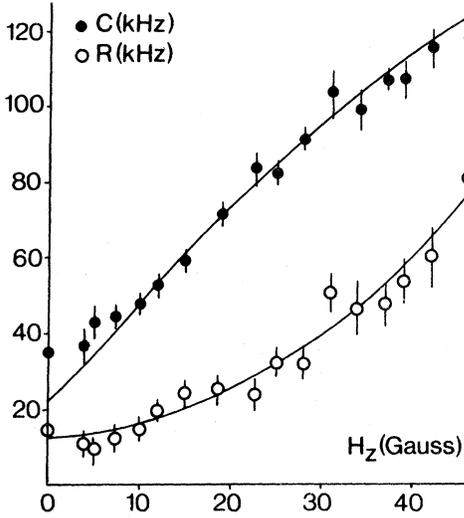
FIG. 9. Magnetic field dependence of $C(z)$ (full circles) and R (open circles) at 1.2 K, when the F_z^{2+}-center spin-echo decay curves are fitted to the form $\exp[-C(z)B(\tau)^{1/2}]$, where $B(\tau)$ is defined by Eq. (2.36c). Drawn curves represent best fits, namely, $C(z) \propto z/(1 + z^2)^{1/2}$ and $R \propto H_z^2$.

phasing is highly unlikely since at the low temperatures of our experiments one would expect spin-lattice relaxation to be controlled by direct (one-phonon) processes leading to $R \propto H_z^4$ for $S = \frac{1}{2}$ spins.[28] On the other hand, it is shown in Appendix B for the special case that exchange is limited to only two subgroups of B spins differing slightly in resonance frequencies, that in the limit of rapid exchange one has

$$R = \frac{\delta^2}{\Gamma + \gamma}, \tag{4.3}$$

where δ is the resonance frequency difference between the subensembles and Γ and γ are explicitly given by (see Appendix B)

$$\Gamma = \pi \sum_{p,p'} \rho_p |\langle fi'p| T(\omega) |if p'\rangle|^2 \delta(\omega_{fi} - \omega_{i'f'} + \omega_{pp'}), \tag{4.4}$$

$$\gamma = \pi \sum_p \rho_p (T_{fi'p, if'p} \Delta T^*_{i'f'} + T^*_{fi'p, if'p} \Delta T_{if}). \tag{4.5}$$

Here p labels the phonon states of density ρ_p and $T(\omega)$ stands for the transition operator.[27,29] Γ and γ denote the homogeneous width of each B-spin packet and the exchange rate due to magnetic dipolar interactions among B spins, respectively. Since in the fraction on the right-hand side of Eq. (4.3) only the numerator is magnetic-field dependent ($\delta \propto H_z$), it follows that the model predicts $R \propto H_z^2$, i.e., the experimentally found effect of

H_z on the B-spin dephasing rate supports the idea that B-spin dephasing arises due to modulated dipolar interactions in the fast exchange limit. This exchange mechanism, which characterizes the system as a T_2 sample, is consistent with the analysis of $T_M(A)$ as a function of temperature.

Let us first focus on Fig. 8, which illustrates the slowing down of the A-spin dephasing as T is increased. Consider now Eq. (2.42) in the following two extreme situations: (i) $R\tau \gg 1$. In this limit the time development of the A-spin echo is approximated by $E(2\tau) \propto \exp[-(2\tau/T_M)^{1/2}]$. From the variation of the parameter x with T in Fig. 8 it is evident that this limiting case, which corresponds to exchange narrowing of the A-B interaction, is never attained. (ii) $R\tau \ll 1$. Now Eq. (2.42) reduces to $E(2\tau) \propto \exp[-(2\tau/T_M)^{3/2}]$, i.e., this functional form of the A-spin echo decay is representative of slow B-spin dephasing as compared to $(M_2^{AB})^{1/2}$, where M_2^{AB} denotes the second moment of the A spins due to magnetic dipolar A-B interaction. Comparison with Fig. 8 shows that the conditions of "slow exchange" for the A-B interactions are gradually approached upon warming the crystal from 1 to 10 K. Apparently, the slowing down of the A-spin dephasing is produced by a decrease in the B-spin dephasing rate R. Such a decrease of R at increasing temperature reflects exchange narrowing within the B-spin ensemble, a phenomenon already arrived at
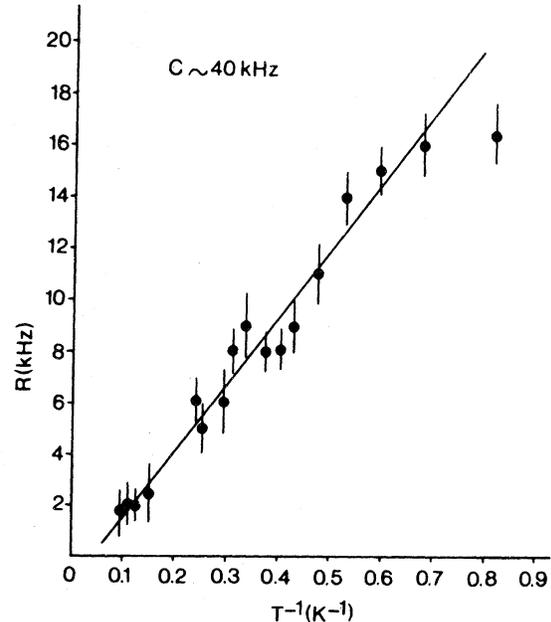
FIG. 10. Spin-dephasing rate (R) of the CaO F^+ centers vs T^{-1} between 1.2 and 10 K. Drawn curve is best fit for $R = 26.2 T^{-1} - 1.1$ kHz.

independently from observed magnetic field effects.

By fitting as before the measured echo decay to the function $\exp[-CB(\tau)]$, but now for different temperatures, we obtain the variation of R as plotted in Fig. 10. It is seen that R appears inversely proportional to temperature. Such a behavior implies within the simple model of two rapidly exchanging B-spin subgroups that Γ and/or γ are linear proportional to temperature. On a series expansion of B-B dipolar spin interactions in phonon coordinates and application of conventional phonon averaging and integration procedures[30] in Eqs. (4.4) and (4.5), one can readily show that in the event of one-phonon assisted exchange Γ and γ become linear proportional to temperature. It is likewise to be expected that in a more rigorous treatment where, in principle, exchange is among transitions with a Gaussian frequency distribution, that the effective rate for one-phonon assisted exchange becomes inversely proportional to temperature as well.

Finally, we comment on the question of why exchange narrowing within the B-spin ensemble occurs at all. The reason is the extremely small inhomogeneous broadening the B-spin ensemble would exhibit when this ensemble is considered in the limit that all dynamical processes are frozen out. This is seen as follows.[8] The numerical analysis of the echo decay curves on the basis of Eq. (2.42) yielded the B-spin density to be $d_B \simeq 10^{17}$ cm^{-3}. As a result, the average dipolar field experienced by each B spin is of the order of ~1 mG. In *zero* field this value would also be representative of the inhomogeneous linewidth since the contribution of strain broadening to the linewidth would be negligible. The latter is inferred from the F^+ center EPR linewidth in X band which was determined as 0.2 G at 4.2 K. Assuming the high-field linewidth to be caused by an inhomogeneous spread (due to strain) in the B-spin g value, one readily extrapolates a residual strain broadening of ~10^{-4} mG in the presence of the local dipolar field. In summary, at zero field or low fields, the inhomogeneous (static) broadening is extremely narrow and therefore readily allows for averaging out by dynamical exchange processes.

C. Spin ordering

In Sec. IV B it was argued from the $x = \frac{3}{2}$ power law for the echo decay that A-spin transitions are not exchange narrowed. This conclusion is confirmed by the determination of the lifetime of the A-spin sublevels by means of spin ordering. As discussed in Sec. II A, the locking of the spin to its own local field is achieved by adiabatic de-

magnetization in the rotating frame (ADRF), while detection of the phenomenon is done by applying a $(\pi/2,0°)$-τ-$(\pi,0°)$-τ'-$(\pi/2,90°)$ modified Hahn-echo cycle.[14]

The building up of coherence along the e_2 axis during the period τ' is representative of the ordering left at time τ_0 after the ADRF sequence. A typical profile, traced optically by the final $(\pi/2,90°)$-probe pulse, is given for the $\tau_z \leftarrow \tau_x$ transition at 1.870 GHz in Fig. 11. The signal was obtained after spin-locking the system during 100 μsec in a H_1 field of 1.8 G; ADRF was completed in 100 μsec, whereas the echo cycle (with $\tau = 2$ μsec) was started at $\tau_0 = 50$ μsec. Using the techniques described in Sec. III, the variation of the peak amplitude of the spin-ordered signal (the maximum occurs for $\tau' = 1.8$ μsec) could be scanned as a function of τ_0. Figure 12 shows the optically detected ordering decay.

The transient decays exponentially with a characteristic time of $T_{ord} = 3.0 \pm 0.3$ msec at temperatures between 1.2 and 4.2 K. As a result, T_{ord} appears to be equal to the lifetime of the radiative τ_z sublevel which was previously determined from
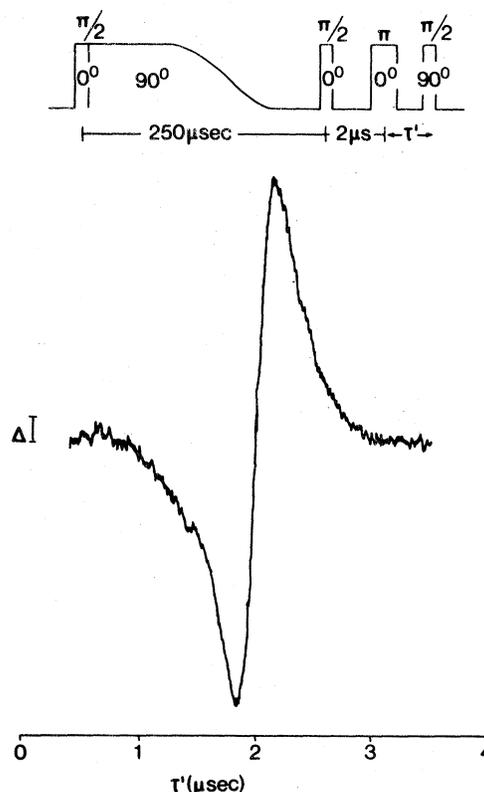
FIG. 11. Optically detected spin-echo in the *ordered* $^3B_1$ state of the $CaOF_2^{2+}$ center as monitored for the $|D-E|$ transition at zero field, $T = 1.2$ K.
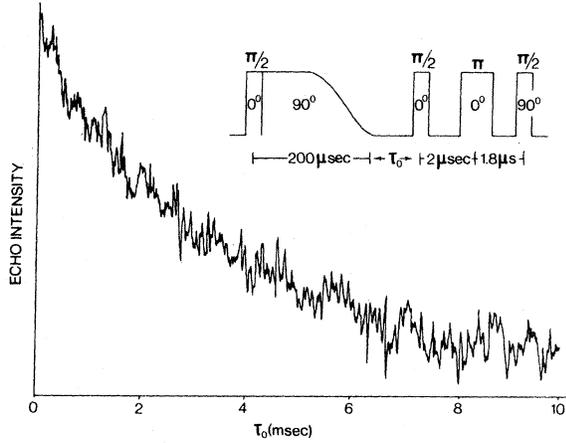
FIG. 12. Optically detected spin-echo decay in the *ordered* $^3B_1$ state of the CaO F_2^{2+} center as monitored for the $|D-E|$ transition at zero field, $T = 1.2$ K.

spin-locking experiments.[7] Furthermore, after nearly complete decay of the τ_z level (at $\tau_0 \simeq 10$ msec) the intensity of the spin-ordered signal was about one-half the initial value (at $\tau_0 \sim 0$), whereas the ordered signal could be followed for still much longer τ_0 values. These data confirm the previous conclusions[7] that the nonradiative level, τ_x, persists much longer than 10 msec without contact through spin-lattice relaxation to the τ_z level. Finally, the results prove unambiguously that near-resonant exchange on a microsecond time scale involving the $^3B_1$ sublevels of the F_2^{2+} center does not occur. Consequently, the observation of the lengthening of the triplet spin-phase memory time (see Sec. IV B) must be attributed to a slowing down of the dephasing of the B spins which act as the stochastic perturbations for the A spins.

V. CONCLUSION

In this paper we studied the role of dynamical spin-spin interactions in the spectral diffusion process for F_2^{2+} centers in their photoexcited $^3B_1$ state. It was demonstrated that dephasing within the ensemble of excited triplet spins (called A spins) results from dipolar coupling to fluctuating $S = \frac{1}{2}$ spins of F^+ centers (which form the B spins).

The applied experimental techniques (optical detection of spin coherence and spin ordering) allowed us to investigate the system in zero or low magnetic fields. Under these circumstances one may reason that the A-B dipolar coupling is suppressed on account of the quenching of the triplet spin magnetic moment in a low-symmetry crystal field. This effect was verified from the magnetic field dependence of the A-spin phase relaxation. Furthermore, at low magnetic fields, one expects a drastic reduction of T_1-type relaxation of the B spins and hence the B-spin precessional motion to dephase predominantly by modulated spin-spin interactions. Support for this hypothesis was obtained from a detailed analysis of the A-spin echo decay curve in the presence of a magnetic field. We find $R \propto H_z^2$ which, as proved for a simplified model, is characteristic of exchange narrowing within the B-spin ensemble.

Coherence measurements as a function of temperature give independent support for this explanation. As the temperature is raised, a decrease of the dephasing rate of the A spins was found. Theoretical and experimental arguments show that the phenomenon is related to a slowing down of the B-spin dephasing ($R \propto T^{-1}$). The interpretation implies the simultaneous effect of spin-spin interactions and spin-phonon coupling of the B spins which results in a one-phonon assisted rapid exchange process.

APPENDIX A

To derive the secular Hamiltonian for dipolar interaction between A ($S=1$) spin and B ($S=\frac{1}{2}$) spins we start with the Hamiltonian for the dipolar interaction between one A and B spin,

$$h_{AB} = \frac{g_A g_B \mu_B^2}{r_{AB}^3} [S_{xA}S_{xB}(1 - 3X_{AB}^2) + S_{yA}S_{yB}(1 - 3Y_{AB}^2) + S_{zA}S_{zB}(1 - 3Z_{AB}^2) - 3(S_{xA}S_{yB} + S_{yA}S_{xB})X_{AB}Y_{AB}$$

$$- 3(S_{yA}S_{zB} + S_{zA}S_{yB})Y_{AB}Z_{AB} - 3(S_{zA}S_{xB} + S_{xA}S_{zB})Z_{AB}X_{AB}]. \tag{A1}$$

The spin operators for the A spin can be expressed in terms of the raising and lowering operators of the α, β, γ basis as follows: Consider the orthonormal set

$$|\alpha\rangle = a_\alpha |+\rangle + b_\alpha |-\rangle,$$

$$|\beta\rangle = a_\beta |+\rangle + b_\beta |-\rangle, \tag{A2}$$

$$|\gamma\rangle = |0\rangle,$$

where $|+\rangle$, $|-\rangle$, and $|0\rangle$ are the $m_s = 1$, -1, and 0 eigenfunctions of the S_z operator. It is readily shown that in the α, β, γ matrix representation one has

$$S_x = \frac{1}{\sqrt{2}} \begin{bmatrix} 0 & 0 & a_\alpha & b_\alpha^* \\ 0 & 0 & a_\beta^* + b_\beta^* \\ a_\alpha + b_\alpha & a_\beta + b_\beta & 0 \end{bmatrix},$$

$$S_y = \frac{1}{i\sqrt{2}} \begin{bmatrix} 0 & 0 & a_\alpha^* - b_\alpha^* \\ 0 & 0 & a_\beta^* - b_\beta^* \\ b_\alpha - a_\alpha & b_\beta - a_\beta & 0 \end{bmatrix}, \qquad \text{(A3)}$$

$$S_z = \begin{bmatrix} a_\alpha^* a_\alpha - b_\alpha^* b_\alpha & a_\alpha^* a_\beta - b_\alpha^* b_\beta & 0 \\ a_\beta^* a_\alpha - b_\beta^* b_\alpha & a_\beta^* a_\beta - b_\beta^* b_\beta & 0 \\ 0 & 0 & 0 \end{bmatrix}.$$

Recalling the matrix representation for the raising and lowering operators $S_{\alpha\beta}$, $S_{\beta\alpha}$, etc. in the α, β, γ basis [see Eq. (2.9)], one obtains from comparison with Eq. (A3)

$$S_x = \frac{1}{\sqrt{2}} [(a_\alpha + b_\alpha)S_{\alpha\gamma} + (a_\alpha^* + b_\alpha^*)S_{\gamma\alpha}$$

$$+ (a_\beta + b_\beta)S_{\beta\gamma} + (a_\beta^* + b_\beta^*)S_{\gamma\beta}],$$

$$S_y = \frac{1}{i\sqrt{2}} [(b_\alpha - a_\alpha)S_{\alpha\gamma} + (a_\alpha^* - b_\alpha^*)S_{\gamma\alpha} \qquad \text{(A4)}$$

$$+ (b_\beta - a_\beta)S_{\beta\gamma} + (a_\beta^* - b_\beta^*)S_{\gamma\beta}],$$

$$S_z = 2a_\alpha^* a_\alpha S_{\alpha\beta} + 2a_\alpha^* a_\beta S_{\beta\alpha} + (a_\alpha^* a_\alpha - b_\alpha^* b_\alpha)S_s,$$

where by definition in the α, β, γ representation

$$S_s = \begin{bmatrix} 1 & 0 & 0 \\ 0 & -1 & 0 \\ 0 & 0 & 0 \end{bmatrix}. \qquad \text{(A5)}$$

It follows that only

$$S_{zA} = (a_\alpha^* a_\alpha - b_\alpha^* b_\alpha)S_{sA} \qquad \text{(A6)}$$

is commutative with $\mathcal{H}_0^A$, and therefore

$$h_{AB}(\text{sec}) = \frac{g_A g_B \mu_B^2}{r_{AB}^3}(a_\alpha^* a_\alpha - b_\alpha^* b_\alpha)S_{sA}S_{zB}(1 - 3Z_{AB}^2),$$

$$\text{(A7)}$$

where it is assumed that H_z is high enough so that the B spin is also quantized along the A-spin principle molecular z axis. For a static magnetic field, H_z, solution of the secular equations yields

$$a_\alpha^* a_\alpha - b_\alpha^* b_\alpha = \frac{z}{(1+z^2)^{1/2}}, \qquad \text{(A8)}$$

in which $z = g_A(H_{loc}^2 + H_z^2)^{1/2}|E|^{-1}$. As a result we obtain

$$h_{AB}(\text{sec}) = \frac{g_A g_B \mu_B^2}{r_{AB}^3} \frac{z}{(1+z^2)^{1/2}} S_{sA}S_{zB}(1 - 3Z_{AB}^2).$$

$$\text{(A9)}$$

APPENDIX B

Here we derive that the correlation function $C_B(t', t)$ is a single exponential decay function for the simplified case of phonon-assisted rapid exchange between two B-spin subgroups with closely spaced spectral transitions $i \rightarrow f$ and $i' \rightarrow f'$, re-

spectively (see also Fig. 13). By definition [cf. Eq. (2.34)]

$$C_B(t', t) = \text{Tr}[\rho\chi(t')\chi^\dagger(t)], \qquad \text{(B1)}$$

where χ equals the B-spin operator. Instead of considering $C_B(t', t)$ directly we find it more convenient to discuss its Fourier pair, $I(\omega)$. The spectral density is given by

$$I(\omega) = \frac{1}{2\pi} \int_{-\infty}^{+\infty} d\tau\, e^{i\omega\tau}\, \text{Tr}[\rho\chi(t)\chi^\dagger]$$

$$= \frac{1}{2\pi} \int_{-\infty}^{+\infty} d\tau\, e^{i\omega\tau}\, \text{Tr}[\rho\chi e^{-i\hat{L}\tau}\chi^\dagger]$$

$$= -\frac{1}{\pi} \text{Im}\, \text{Tr}[\rho\chi G(\omega)\chi^\dagger]. \qquad \text{(B2)}$$

In Eq. (B2) use was made of the Liouvillian L, which operates in Liouville space as[19]

$$\rho(t) = e^{-i\hat{L}t}\rho(0), \qquad \text{(B3)}$$

and the Green-function operator in Liouville space defined by

$$G(\omega) = \frac{1}{\omega - L}. \qquad \text{(B4)}$$

To evaluate matrix elements of $G(\omega)$ we follow the procedure of Ref. 27. There it was argued that $I(\omega)$ of Eq. (B2) can be rewritten as

$$I(\omega) = -\frac{1}{\pi} \text{Im} \left\langle\!\left\langle \chi^\dagger \rho^s \left| \frac{1}{\omega - L_0 - \langle t \rangle} \right| \chi^\dagger \right\rangle\!\right\rangle, \qquad \text{(B5)}$$

where the double angular brackets indicate representation in Liouville space, $\rho = \rho^s \rho^b$ where ρ^s and ρ^b denote the density operators for the B spin and bath states, respectively, L_0 is the Liouvillian for the ensemble of isolated B spins and $\langle t \rangle$ is the thermal average of the full transition superoperator where the latter satisfies

$$t = L_1 + L_1 G_0 t, \qquad \text{(B6)}$$

in which L_1 denotes the Liouvillian representative
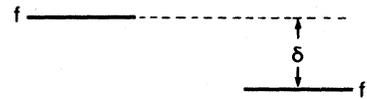
FIG. 13. Illustration of the level scheme for one-phonon assisted exchange between two nonresonant B spins.

for the interactions of the B spins with themselves and the phonon bath. For the case of interest here, namely exchange between if and $i'f'$ transitions, the Liouville space is spanned by

$$|if\rangle\rangle = |ii'p\rangle\langle fi'p|$$

and   (B7)

$$|i'f'\rangle\rangle = |ii'p'\rangle\langle if'p'|\,,$$

where the Hilbert operators operate in the product space formed by the eigenstates of the two exchanging B spins (see also Fig. 13) and the phonon state vectors.

For simplicity we take $\langle f|\chi|i\rangle = \langle f'|\chi|i'\rangle = \chi_{fi}$ and also we assume that initially only the i and i' states are occupied in the otherwise incoherent

$$\{g\} = \begin{bmatrix} \omega - \omega_0 - \delta_{22} + i\Gamma_{22} & \delta_{12} + i\gamma_{12} \\ \delta_{21} + i\gamma_{21} & \omega - \omega_0 - \delta_{11} + i\Gamma_{11} \end{bmatrix} \Big/ \mathrm{Det}\,|g^{-1}|\,.$$ (B10)

As discussed in Refs. 27 and 29, Γ_{kl} and γ_{kl} can be expressed in terms of matrix elements of the transition operator in Hilbert space. We obtain after an elaborate calculation in the limit that $\omega \simeq \omega_{fi} \simeq \omega_{f'i'}$

$$\Gamma_{11} = \pi \sum_{p,\,p'\,;kk'p'\neq f\,i'\,p} \rho_p |\langle fi'p|T(\omega_1)|kk'p'\rangle|^2 \delta(\omega_{fk} - \omega_{k'i'} + \omega_{pp'})$$

$$+ \pi \sum_{p,p'\,;kk'p'\neq i\,i'p} \rho_p |\langle ii'p|T(\omega_2)|kk'p'\rangle|^2 \delta(\omega_{ik} - \omega_{k'i'} + \omega_{pp'})$$

$$+ \pi \sum_{p,\,p'} \rho_p |\langle fi'p|T(\omega_1)|fi'p'\rangle - \langle ii'p|T(\omega_2)|ii'p'\rangle|^2 \delta(\omega_{pp'})\,,$$ (B11)

where $\omega_1 = \omega_f + \omega_{i'} + \omega_p$, $\omega_2 = \omega_i + \omega_{i'} + \omega_p$, and $T(\omega)$ equals the transition operator in Hilbert space which satisfies

$$T = V + VG_0 T\,.$$ (B12)

Here V includes terms that represent the magnetic dipolar interaction between the exchanging spins as well as the spin-phonon coupling for each separate B spin.

Under the assumption that all *intra*molecular relaxation processes (of T_1 and T_2 type) can be excluded we obtain for Γ_{11}

$$\Gamma_{11} \simeq \pi \sum_{p,\,p'} \rho_p |\langle fi'p|T(\omega_1)|if'p'\rangle|^2 \delta(\omega_{fi} - \omega_{f'i'} + \omega_{pp'})\,.$$ (B13)

This expression is contained in the first summation on the right-hand side of Eq. (B11) and represents the broadening of the if transition due to exchange between $|1\rangle\rangle$ and $|2\rangle\rangle$. Within the same approximation Γ_{22} can be calculated. The result is $\Gamma_{22} = \Gamma_{11} \equiv \Gamma$.

Similarly, we find

B-spin ensemble: $\rho^s = \rho_i^s \rho_{i'}^s$. With these assertions Eq. (B5) is reduced to

$$I(\omega) = -\frac{1}{\pi}\,\rho_i^s\rho_{i'}^s\,|\chi_{fi}|^2\,\mathrm{Im}\sum g_{ab,\,cd}\,,$$ (B8)

where $g_{ab,\,cd} = \langle\langle ab|g|cd\rangle\rangle$, $g = (\omega - L_0 - \langle t\rangle)^{-1}$, and the summation is over all possible (four) matrix elements using the set of (B7).

Consider now the matrix $\{g\}$ in the (1, 2) basis using the notation $|1\rangle\rangle = |if\rangle\rangle$ and $|2\rangle\rangle = |i'f'\rangle\rangle$:

$$\{g\} = \begin{bmatrix} \omega - \omega_{f'i'} - \langle t\rangle_{22} & \langle t\rangle_{12} \\ \langle t\rangle_{21} & \omega - \omega_{fi} - \langle t\rangle_{11} \end{bmatrix} \Big/ \mathrm{Det}\,|g^{-1}|\,,$$ (B9)

where $\mathrm{Det}\,|g^{-1}|$ stands for the determinant of the g^{-1} matrix. Introduce

$$\gamma_{12} \simeq \gamma_{21} \equiv \gamma = \pi \sum_p \rho_p T_{fi'p,\,if'\,p}(T^*_{ii'p,\,ii'p} - T^*_{if'p,\,if'p})$$

$$+ T^*_{fi'p,\,if'p}(T_{ii'p,\,ii'p} - T_{fi'p,\,fi'p})\,.$$ (B14)

Note that off-diagonal elements in $\{g\}$ occur only if the magnetic dipolar interaction simultaneously effects exchange and anisotropy in the scattering by the B spins. With the aforementioned assumptions and neglect of the exchange-induced shifts in the resonance frequency, $\{g\}$ can be written as

$$\begin{bmatrix} \omega - \omega_0 + \delta + i\Gamma & i\gamma \\ i\gamma & \omega - \omega_0 - \delta + i\Gamma \end{bmatrix} \Big/ \mathrm{Det}\,|g^{-1}|\,,$$

where $\delta = (\omega_{fi} - \omega_{f'i'})/2$. Assuming the limit of rapid exchange, i.e., $\gamma^2 \simeq \Gamma^2 \gg \delta^2$ one can finally show that $I(\omega)$ approaches

$$I(\omega) \propto \frac{\delta^2/(\Gamma+\gamma)}{(\omega - \omega_0)^2 + [\delta^2/(\Gamma+\gamma)]^2}\,.$$ (B15)

Equivalently, the autocorrelation function which is the Fourier transform of $I(\omega)$ is obtained as

$$C_B(t',t) \propto \exp(-R|t'-t|)\,,$$ (B16)

where the dephasing rate R is given by

$$R = \delta^2/(\Gamma+\gamma)\,.$$ (B17)

[1]W. B. Mims, K. Nassau, and J. D. Mc Gee, Phys. Rev. **123**, 2059 (1961).

[2]For a review, see *Time Domain Electron Spin Resonance*, edited by L. Kevan and R. N. Schwartz (Wiley, New York, 1979).

[3]W. B. Mims, in *Electron Paramagnetic Resonance*, edited by S. Geschwind (Plenum, New York, 1972), p. 263.

[4]See, e.g., the contribution by J. Schmidt and J. H. van der Waals in Ref. 2, p. 343.

[5]W. G. Breiland, H. C. Brenner, and C. B. Harris, J. Chem. Phys. **62**, 3458 (1975).

[6]D. J. Gravesteijn, J. H. Scheijde, and M. Glasbeek, Phys. Rev. Lett. **39**, 105 (1977).

[7]D. J. Gravesteijn and M. Glasbeek, Phys. Rev. B **19**, 5549 (1979).

[8]M. Glasbeek, R. Hond, and A. H. Zewail, Phys. Rev. Lett. **45**, 744 (1980).

[9]G. W. Leppelmeier and E. L. Hahn, Phys. Rev. **141**, 724 (1966).

[10]M. Schwab and E. L. Hahn, J. Chem. Phys. **52**, 3152 (1970).

[11]A. Abragam, *The Principles of Nuclear Magnetism* (Clarendon, Oxford, 1961).

[12]R. P. Feynman, F. L. Vernon, Jr., and R. W. Hellwarth, J. Appl. Phys. **28**, 49 (1957).

[13]C. P. Slichter and W. C. Holton, Phys. Rev. **122**, 1701 (1961).

[14]H. C. Brenner, J. C. Brock, and C. B. Harris, J. Chem. Phys. **60**, 4448 (1974).

[15]J. C. Brock and C. B. Harris, Chem. Phys. **43**, 55 (1979).

[16]J. R. Klauder and P. W. Anderson, Phys. Rev. **125**, 912 (1962).

[17]W. B. Mims, Phys. Rev. **168**, 370 (1968).

[18]P. Hu and S. R. Hartmann, Phys. Rev. B **9**, 1 (1974).

[19]R. W. Zwanzig, *Lectures in Theoretical Physics* (University of Colorado, Boulder, Colorado, 1960), Vol. 3, p. 106; H. Mori, Prog. Theor. Phys. (Kyoto) **33**, 423 (1965).

[20]See, e. g., B. J. Berne and G. D. Harp, in *Advances in Chemical Physics*, edited by I. Prigogine and S. A. Rice (Interscience, New York, 1970), Vol. 17, p. 63.

[21]See, e. g., M. Mehring, *High Resolution* NMR *Spectroscopy in Solids* (Springer, Berlin, 1976), p. 227.

[22]U. Haeberlen, *High Resolution* NMR *in Solids, Selective Averaging*, Suppl. I to Advances in Magnetic Resonance (Academic, New York, 1976), p. 67.

[23]R. Hond and M. Glasbeek (unpublished).

[24]P. W. Anderson and P. R. Weiss, Rev. Mod. Phys. **25**, 269 (1953); P. W. Anderson, J. Phys. Soc. Jpn. **9**, 316 (1954).

[25]See, e. g., Ref. 11, p. 126.

[26]The pulse sequence generator was designed and built by J. H. Scheijde of our laboratory; J. H. Scheijde (unpublished).

[27]K. E. Jones and A. H. Zewail, in *Advances in Laser Chemistry*, Proceedings of the Conference on Advances in Laser Chemistry, California Institute of Technology, Pasadena, 1978, Vol. 3 of *Springer Series of Chemical Physics*, edited by A. H. Zewail (Springer, New York, 1978), p. 196.

[28]J. H. Van Vleck, Phys. Rev. **57**, 426 (1940).

[29]A. Ben-Reuven, in *Advances in Chemical Physics*, edited by I. Prigogine and S. A. Rice (Wiley, New York, 1975), Vol. 33, p. 235.

[30]R. Orbach and H. J. Stapleton, in *Electron Paramagnetic Resonance*, edited by S. Geschwind (Plenum, New York, 1972), p. 121.